







Performance comparison of permafrost models in Wudaoliang Basin, Qinghai-Tibet Plateau, China

YIN Guo-an^{1,2}  <http://orcid.org/0000-0002-8855-8388>; e-mail: yinguoan123@126.com

NIU Fu-jun¹  <http://orcid.org/0000-0003-0524-2618>;  e-mail: niufujun@lzb.ac.cn

LIN Zhan-ju¹  <http://orcid.org/0000-0001-6557-9998>; e-mail: zhanjulin@lzb.ac.cn

LUO Jing¹  <http://orcid.org/0000-0002-8737-6646>; e-mail: luojinabcd@163.com

LIU Ming-hao^{1,2}  <http://orcid.org/0000-0002-0093-0588>; e-mail: liuminghao@lzb.ac.cn

¹ State Key Laboratory of Frozen Soils Engineering, Cold and Arid Regions Environmental and Engineering Research Institute, Chinese Academy of Sciences, Lanzhou 730000, China

² University of Chinese Academy of Sciences, Beijing 100049, China

Citation: Yin GA, Niu FJ, Lin ZJ, et al. (2016) Performance comparison of permafrost models in Wudaoliang Basin, Qinghai-Tibet Plateau, China. *Journal of Mountain Science* 13(7). DOI: 10.1007/s11629-015-3745-x

© Science Press and Institute of Mountain Hazards and Environment, CAS and Springer-Verlag Berlin Heidelberg 2016

Abstract: Knowledge of the spatial distribution of permafrost and the effects of climate on ground temperature are important for land use and infrastructure development on the Qinghai-Tibet Plateau (QTP). Different permafrost models have been developed to simulate the ground temperature and active layer thickness (ALT). In this study, Temperature at Top of Permafrost (TTOP) model, Kudryavtsev model and modified Stefan solution were evaluated against detailed field measurements at four distinct field sites in the Wudaoliang Basin to better understand the applicability of permafrost models. Field data from 2012 to 2014 showed that there were notable differences in observed ground temperatures and ALTs within and among the sites. The TTOP model is relatively simple, however, when driven by averaged input values, it produced more accurate permafrost surface temperature (Tps) than the Kudryavtsev model. The modified Stefan solution resulted in a satisfactory accuracy of 90%, which was better than the Kudryavtsev model for estimating ALTs. The modified Stefan solution had the potential of being applied to climate-change studies in the future.

Received: 12 October 2015
Revised: 17 December 2015
Accepted: 10 March 2016

Furthermore, additional field investigations over longer periods focusing on hydrology, which has significant influence on permafrost thaw, are necessary. These efforts should employ advanced measurement techniques to obtain adequate and extensive local parameters that will help improve model accuracy.

Keywords: Permafrost model; Active layer thickness; Soil freeze-thaw; Soil temperature

Introduction

Approximately one quarter of the northern hemisphere is underlain by permafrost (Wu and Zhang 2008; Zhang et al. 1999), which is defined as the ground that remains at or below 0°C for two or more continuous years (Van Everdingen 1998). The IPCC Fifth Assessment Report (Vaughan et al. 2013) indicates that most permafrost has been degrading since the little ice age and the rate has increased recently as evidenced by permafrost temperature increasing and positive trend of the active layer thickness. Permafrost degradation has impacted

surface and subsurface hydrologic conditions, soil strength properties and ecosystems (Kurylyk et al. 2014a).

In China, permafrost regions occupy a significant portion of the land area, however, the permafrost coverage is estimated to have been reduced by about 18.6% since the late 1980s (Cheng and Jin 2013). Permafrost in China is mainly found on the Qinghai-Tibet Plateau (QTP), the largest lower latitude permafrost region in the world. Permafrost on the QTP is thinner and warmer than that in the polar regions of, for example, North America and Russia. Recent climate warming has been recorded on the QTP (Xie et al. 2012), and the trend is greater than the global average (Yang et al. 2010). Permafrost is sensitive to climate change and environmental disturbances because it is the product of interactions between the earth-atmosphere system (Henry and Smith 2001; Smith and Riseborough 1996, 2002). On the QTP, the climate warming causes increases in ground temperatures, active-layer thicknesses (ALT), and the initiation of thermokarst processes (Ding 1998; Jin et al. 2006; Wang 1993). These changes may affect the infrastructure stability of the Qinghai-Tibet Railway (QTR) and the Qinghai-Tibet Highway (QTH). Recent studies indicate that the rate of ALT increase along the QTR (7.8 cm yr^{-1}) is higher than it in other regions of the QTP (1.33 cm yr^{-1}) (Wu and Zhang 2010; Zhao et al. 2010). Concurrently, increases in permafrost temperature have markedly changed the cold-regions hydrogeology on the QTP (Cheng and Jin 2013). Therefore, mapping the distribution of permafrost and determining potential changes caused by climate warming are important for land use planning, infrastructure development, and ecological and hazard assessments.

Different permafrost models have been developed to map permafrost at various scales in arctic and mountain regions. These models may be of the equilibrium, empirical-statistical, or process-based types and have been widely used at regional and local scales (Riseborough et al. 2008; Harris et al. 2009). Field measurements are difficult to obtain in more remote areas on the QTP, so permafrost models are useful for examining changes under climate warming scenarios. Li and Cheng (1996) used analytical methods and

numerical simulations to examine permafrost evolution and ground temperature variations on the QTP. Later, Li and Cheng (1999) predicted changes to permafrost at different altitudes using a model integrated with a geographic information system. Luo et al. (2014) applied the Kudryavtsev model to simulate the ALT and changes to ground temperatures in the source area of the Yellow River. These limited studies described permafrost conditions at a broad scale, but did not account for complex topography and vegetation patterns or hydrogeological processes at the surface and within the active layer. Therefore, these were large-scale approximations in infrastructure risk assessment. More research using permafrost models should be carried out on the QTP at a finer spatial scale.

Given the proposed power transmission line, expressway, and oil/gas pipeline in the Qinghai-Tibet Engineering Corridor (QTEC), additional knowledge of permafrost distribution and its relationships with geomorphology is needed. The active layer plays a significant role in the surface energy balance, hydrologic cycle, carbon exchange between the atmosphere and the land surface, local ecosystem, and human infrastructure (Wu and Zhang 2010). Therefore, it is necessary to determine the active-layer thickness quickly and accurately.

To examine the applicability of different models on the QTP, we tested four analytical models to simulate the ALT and the ground temperatures in Wudaoliang Basin, located in central QTP. The objectives of this study were: (1) to calculate the mean annual temperature at the permafrost surface (T_{ps}) and active layer thickness (ALT) at the study sites, (2) to compare these results with field measurements, and (3) to evaluate the applicability of these models.

1 Study Area and Data Acquisition

1.1 Sites description

Four field measurement sites (1 to 4) were situated in Wudaoliang Basin (35.19° E , 93.08° N) about 280 km from Golmud (Figure 1). The average elevation in the region is about 4616 m. The study area is characterized by flat terrain and arid soils with continuous permafrost (Fang et al.

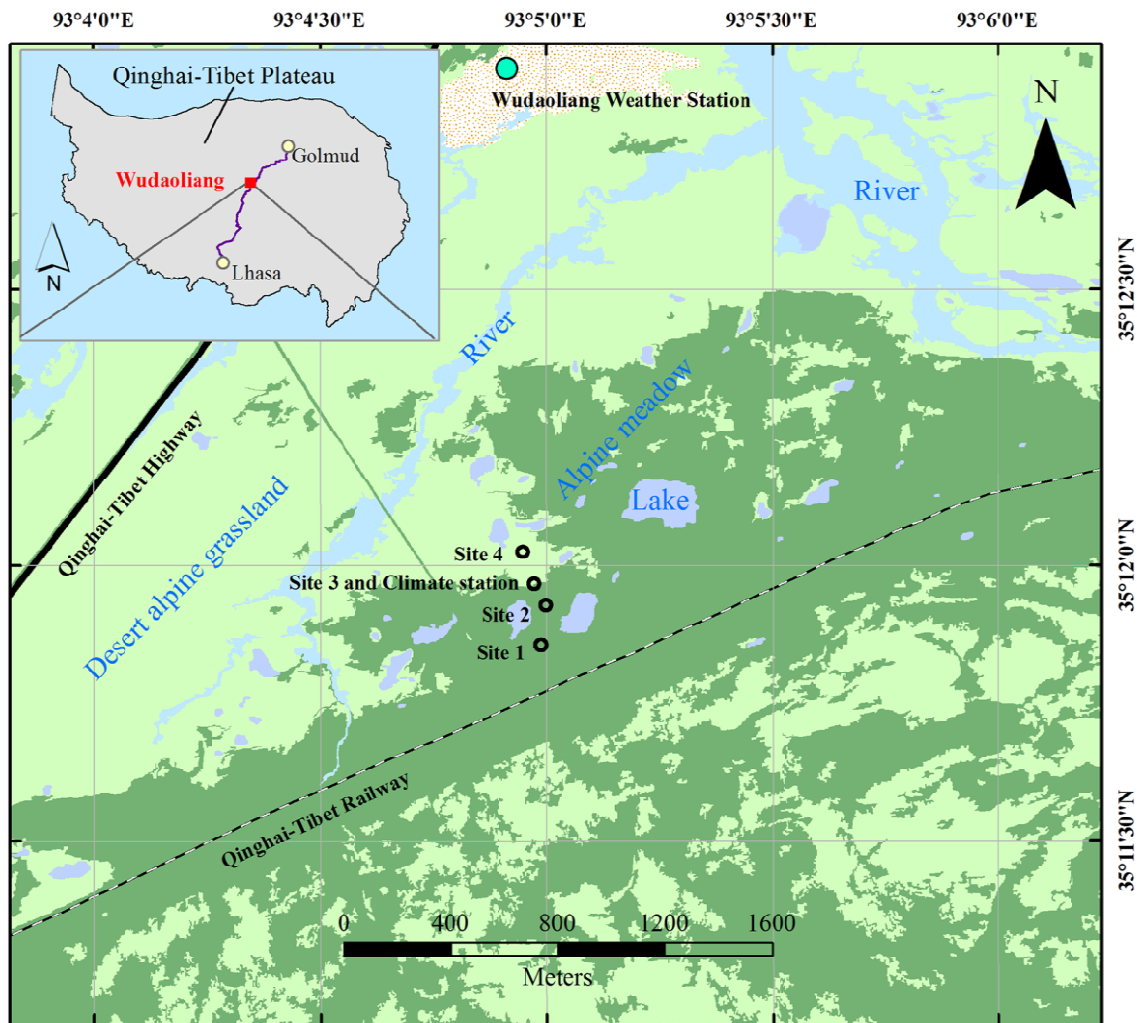


Figure 1 Overview of the field sites in the Wudaoliang Basin over the Qinghai-Tibet Plateau. Black circles present four field sites with different ground surface. This map based on the image of GF-1, a satellite launched by China in 2013, shows two major ground surface types. The site 1 is located in alpine meadow area with rock grid, site 2 is in the alpine meadow area. Site 3 is in the grassland- meadow transition area and the climate is beside it. Site 4 situates in the desert alpine grassland. The green solid dot on the top indicates the Wudaoliang Weather Station. The satellite data is available at <http://218.247.138.121/DSSPlatform/productSearch.html>.

2015; Jin et al. 2008). The Wudaoliang Weather Station, operated by State Meteorological Administration, China, is about 2 km from the field sites and provides atmospheric data from 1957 to present. The mean annual air temperature (MAAT) was about -4.5°C between 2000 and 2013. Air temperatures have been rising at 0.03°C per decade (Figure 2). Mean annual precipitation was 218 mm to 358 mm, and annual evaporation was about 1421 mm. Snow cover is commonly an important factor regulating ground temperatures. However, we observed little or no persistent snow cover in Wudaoliang Basin. The ground surface types at the sites are shown in Figures 1 and 3. Site

1 is characterized by alpine meadow with a rock grid to protect the railway roadbed from blowing sands. Site 2 is located in alpine meadow. Site 3 is in a transition area between alpine meadow and desert grassland. Site 4 is in desert grassland area. The site conditions represented four common ecological communities on the QTP. All sites were underlain by ice-rich permafrost (Lin et al. 2015).

Sixty boreholes were drilled in August 2010 (15 boreholes at each site) to monitor ground temperatures from the surface to 5 m depth and to determine the ALT. The separation between each borehole was 5 m, forming a $10\text{ m} \times 20\text{ m} \times 5\text{ m}$ three-dimensional grid at each site. Thermistor

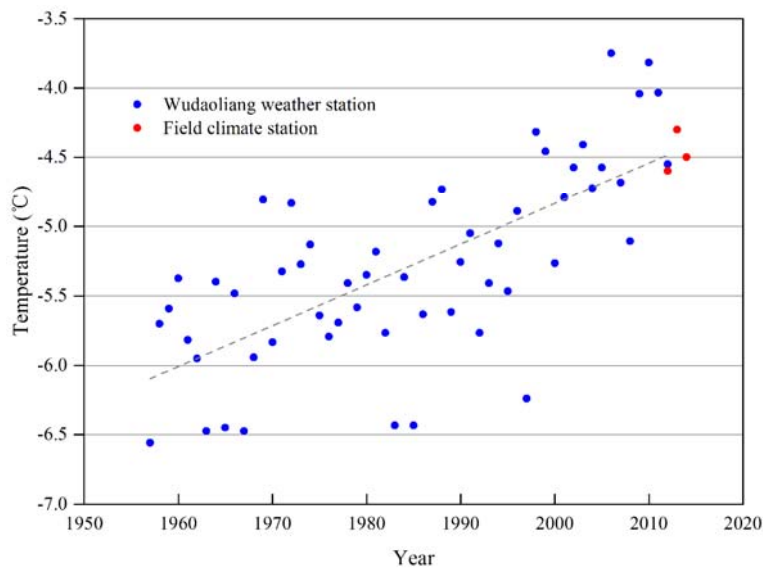


Figure 2 Mean annual air temperatures from the Wudaoliang Weather Station and the climate station in our study sites (Field climate station). Data from the Wudaoliang Weather Station was from 1957 to 2012 (blue dots, $R^2=0.5$). Data from the climate station in our study sites was from 2012 to 2014 (red dots, $R^2=0.1$).



Figure 3 Geomorphic conditions of the four field sites. A (Site 1): alpine meadow with rock grid and high vegetation coverage ($\geq 60\%$). B (Site 2): alpine meadow with high vegetation coverage ($\geq 60\%$). C (Site 3): transitional area between alpine meadow and grassland with moderate vegetation coverage (45% to 60%). D (Site 4): alpine grassland with low vegetation coverage (10% to 30%). Each site covers about 200 m². The pictures were taken in August 2014.

cables with 23 sensors ($\pm 0.02^\circ\text{C}$ accuracy) were installed in each borehole with a PVC pipe for sensor housing. The thermistor spacing was 0.05 m within the upper 0.3 m, 0.1 m between 0.3 and 0.5 m, 0.25 m between 0.5 and 3 m, and 0.5 m below 3 m. At each site, three Onset Soil Moisture Smart

Sensors with the resolution of 0.0007 m³/m³ (0.07%), were placed at 0.5 m, 1.0 m, and 1.5 m depth in August 2010. The soil moisture instruments failed at Site 2, so reported results are limited to Sites 1, 3, and 4. The data acquisition system at each site consisted of a Campbell Scientific CR3000 data logger powered by solar panels and batteries. Data collection at the four sites began in July 2011 with measurements recorded every four hours. An Onset HOBO weather station was installed near Site 3 in July 2010. Air temperature was measured every 30 minutes at 2 m above the ground surface in an unventilated radiation shield. Precipitation, wind speed and direction, solar radiation, and ground temperature at 0.1 m below the surface were also recorded every 30 minutes. All data from 2012 to 2014 are analyzed in this paper.

1.2 Soil properties

During the borehole drilling in summer 2010, we collected the soil samples from each site for property analysis. Gravimetric water content (ω) was calculated from mass lost after drying the soil. Bulk density (ρ) was also determined with the cutting-ring method. Soil descriptions were taken in order to determine soil type and distribution profiles. The thermal conductivity (K) and heat capacity (C) of surface soil were determined from Xu et al. (2010). Soil parameters from boreholes used in the model parameterization are summarized in Table 1. Each soil parameter was averaged in one soil layer.

2 Modeling Methods

In this study, four analytical equations were used to calculate ALT and T_{ps} at the field sites. We

Table 1 Soil profiles, ground surface type and soil thermal properties of four sites (from 0.05 m in depth to the permafrost surface)

Sites	Vegetation type	Soil type	Thickness (m)	Soil water content ω^* (%)	Dry density ρ (kg/m ³)	Thermal conductivity* (W/ (m °C))		Volumetric heat capacity* (kJ/ m ³ °C)	
						K_t	K_f	C_t	C_f
1	Alpine meadow with rock grid	Fine sand	1.80	16.5	1400	1.31	1.53	1288.5	1158.0
		Sand loam	1.00	16.4	1480	0.91	0.96	1447.1	1257.6
2	Alpine meadow	Fine sand	1.90	14.1	1540	1.37	1.42	1388.1	1247.6
		Sand loam and gravel	0.60	23.0	1500	1.14	1.31	1217.1	1086.7
3	Transitional zone	Fine sand	1.70	15.5	1450	1.26	1.49	1323.1	1189.1
		Sand loam and gravel	0.80	16.5	1570	1.03	1.17	1536.4	1371.8
4	Desert Grassland	Fine sand	1.70	10.8	1574	1.37	1.68	1377.8	1238.2
		Red clay	0.90	15.2	1840	1.16	1.39	1551.2	1421.9

Notes: ※ Values converted from Xu et al. (2010); *Averaged value for one soil layer; Soil water content, volumetric heat capacity, density and volumetric heat capacity were averages of each soil layer.

choose the methods based on the parameters required, and satisfactory performance of the models in other recent studies. The symbols used in the equations are listed in Table 2.

2.1 Equations for temperature at the permafrost surface

Smith and Riseborough (1996, 2002) estimated the mean annual temperature at the permafrost surface (T_{ps}) with the TTOP model (Eq. 1), which combines the thermal offset with ground surface freezing and thawing indices. This model assumes that the relationship between ground surface temperature and temperature at the permafrost surface is determined primarily by conductive heat flow. T_{ps} can be regarded as the result of the interaction between the air temperature regime, surface offset, and the thermal offset. The detailed derivation of this model can be found in Smith and Riseborough (2002). In this paper, we used the surface temperature, rather than the air temperature, as the driving variable.

$$TTOP = \frac{K_t DDT_s - K_f DDF_s}{K_f P} \quad (1)$$

Kudryavtsev et al. (1977) showed that T_{ps} could be calculated using a semi-empirical and analytical equation:

Table 2 Symbols used in predictive equations

Symbol	Description	Units
DDT_s	Thawing index for ground surface temperature (degree-days)	°C·days
DDF_s	Freezing index for ground surface air temperature (degree-days; expressed as a positive number)	°C·days
P	Annual period (365 days)	Days
K_t	Thermal conductivity of thawed ground	W/ (m °C)
K_f	Thermal conductivity of frozen ground	W/ (m °C)
C_t	Volumetric heat capacity of thawed ground	kJ/ m ³ °C
C_f	Volumetric heat capacity of frozen ground	kJ/ m ³ °C
A_s	Amplitude of annual temperature variations at soil surface	°C
T_s	Mean annual temperatures at the ground surface	°C
L	Latent heat (334) (Xu et al. 2010)	kJ/kg
ρ	Dry density of soil	kg/m ³
ω	soil water content by weight	-
Z	The maximum thaw depth (ALT)	m

$$T_{ps} = \frac{0.5T_s (K_f + K_t) + A_s \frac{K_t - K_f}{\pi} \left[\frac{T_s}{A_s} \arcsin \frac{T_s}{A_s} + \sqrt{1 - \frac{T_s^2}{A_s^2}} \right]}{K_f} \quad (2)$$

This equation determines the mean annual ground temperature by consecutively introducing the thermal effects of snow, ground surface vegetation, and active-layer soils layer by layer, so that temperatures and seasonal amplitudes are defined at each level (snow surface, vegetation surface, ground and permafrost surfaces) (Sazonova and Romanovsky 2003).

2.2 Equations for active layer thickness

2.2.1 Modified Stefan solution

A number of simplified analytical solutions have been proposed to calculate ALT. One of the simplest is the Stefan equation. However, the standard Stefan equation always overestimates the thaw depth because the heat capacity is not considered. A modified Stefan equation (Eq. 3a) was proposed by several researchers, and Kurylyk and Masaki (2015) presented improved Stefan equation correction factors that account for the influence of soil heat capacity.

$$\begin{aligned}
 Z &= \lambda \sqrt{\frac{2K_i DDT_s}{\rho\omega L}} & (a) \\
 S_{T_1} &= \frac{C_u T_s}{\rho\omega L} & (b) \\
 \lambda_s &= 1 - 0.16S_{T_1} + 0.038S_{T_1}^2 \quad (T_i = 0 \text{ }^\circ\text{C}) & (c) \\
 \lambda_6 &= \left[1 + 0.147S_{T_1} \left(\beta \frac{T_i}{T_s} \right)^2 + 0.535\sqrt{S_{T_1}} \beta \frac{T_i}{T_s} \right] \times \lambda_s \quad (T_i < 0 \text{ }^\circ\text{C}) & (d) \\
 \beta &= \sqrt{\frac{K_f C_f}{K_i C_u}} & (e)
 \end{aligned}
 \tag{3}$$

where λ is a dimensionless correction factor which is less than 1 with the form of Eq. 3c or 3d. S_{T_1} is the Stefan number with the form of Eq. 3b when the T_s is a constant value. T_i is the initial temperature during thawing. β is a dimensionless parameter that accounts for differences in soil thermal properties, which can be assumed to be 1 for most soils (Kurylyk and Masaki 2015). More general discussion of these equations are found in Kurylyk and Masaki (2015) and Kurylyk et al. (2014b).

2.2.2 Kudryavtsev model

Romanovsky and Osterkamp (1997) estimated the ALT in Alaskan using several years of field data with the standard Stefan equation and the Kudryavtsev equation (Eq. 4), which accounted for heat fluxes and phase changes (Kudryavtsev et al. 1977). The Kudryavtsev equations overestimated the ALT by an average of 2 cm, less than the 13 cm error for the standard Stefan equation. Sazonova and Romanovsky (2003) applied these equations to develop the model GIPL 1.0. One disadvantage of Eq. 4 is that T_{ps} is required as an input. In this paper, we refer to Eq. 2 and Eq. 4 as the Kudryavtsev model.

$$Z = \frac{2(A_s - T_{ps})\sqrt{\frac{K_i C_i P}{\pi}} + \frac{(2A_2 C_i X_c + \rho L X_c)L\sqrt{\frac{K_i P}{\pi C_i}}}{2A_2 C_i X_c + \rho L X_c + (2A_2 C_i + \rho L)\sqrt{\frac{K_i P}{\pi C_i}}}}{2A_2 C_i + \rho L}$$

where,

$$A_2 = \frac{A_s - T_{ps}}{\ln\left(\frac{A_s + \rho L / 2C_i}{T_{ps} + \rho L / 2C_i}\right)} - \frac{\rho L}{2C_i}, \quad \text{and} \quad X_c = \frac{2(A_s - T_{ps})\sqrt{\frac{K_i C_i P}{\pi}}}{2A_2 C_i + \rho L}
 \tag{4}$$

The Kudryavtsev model assumes thermal equilibrium, which means that temperature averages over decades rather than a single year should be used as input. However, only 3 years of ground temperature and air temperature data are available from this study. Figure 2, based on long-term climate data from the Wudaoliang Weather Station, indicates that the 3 years for this study were not extremely warm or cold. Therefore, we considered that these data were appropriate despite the model assumption (Wilhelm et al. 2015).

3 Results

3.1 Field measurements

Mean annual ground surface temperatures (T_s) from a depth of 0.05 m was calculated for each site at the 15 boreholes (Figure 4). During the study period, T_s values exhibited notable intra-site

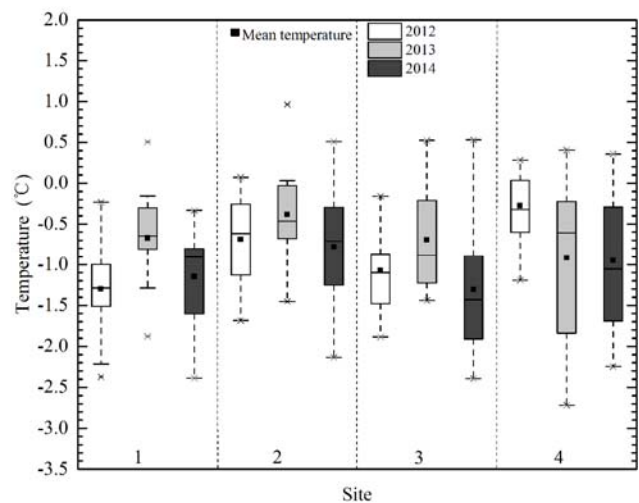


Figure 4 Box plots of mean annual ground surface temperature at a depth of 0.05 m for each year of the field sites.

variability. Hence, the temperatures were each averaged for all 15 boreholes at each site from 2012 to 2014 (i.e. 3-year mean value) to eliminate the variations. ALT was determined by identifying the maximum seasonal penetration of the 0°C isotherm from the thermistor cable data. T_{ps} was calculated from the sensors closest to the bottom of the active layer. Figure 5 presents the measured values for each prediction equation during the study period. For all sites, T_s ranged from -1.1°C to -0.6°C. The mean annual T_{ps} ranged between -1.8°C at site 1 and -0.5°C at site 4, with SD (standard deviation) values below 0.37°C. At site 4, both T_s and T_{ps} were higher than at the other sites. The mean annual degree days were ranged from 1101°C·days to 1235°C·days for thawing periods (DDT_s) and 1373°C·days to 1559°C·days for freezing periods (DDF_s). There were little differences of DDT_s among the sites. The ALT for all sites ranged from 1.70 m to 2.54 m, with SD values lower than 0.31 m. The mean temperature at the ground surface was 6.2°C to 6.8°C during the thawing period for all sites. Average annual surface temperature amplitudes (A_s) for the four sites was about 10.6°C.

3.2 Permafrost surface temperature modeling

Table 3 summarizes the statistical analysis of simulated T_{ps} from Eq. 1 and Eq. 2, and the measured values at the four sites. Eq. 1 is a simple algorithm that requires the mean annual degree days (DDT_s , DDF_s) and soil thermal properties. Furthermore, it seems that Eq. 1 performed satisfactorily simulations at all sites with the mean relative error below 24%. The T_{ps} values from Eq. 1 were always higher than the measured values, with the differences ranging from 0.02°C to 0.43°C. Eq. 2 accounted for the seasonal amplitudes, and produced lower simulated T_{ps} than the measured values, with the differences between 0.15°C and 0.25°C. The mean relative error of Eq. 2 was estimated below 30% for all sites.

3.3 Active layer thickness modeling

The ALTs at the four sites were calculated using the measured parameters for Eq. 3 and Eq. 4. Comparisons of the calculated and measured ALTs are shown in Figure 6 and a statistical analysis

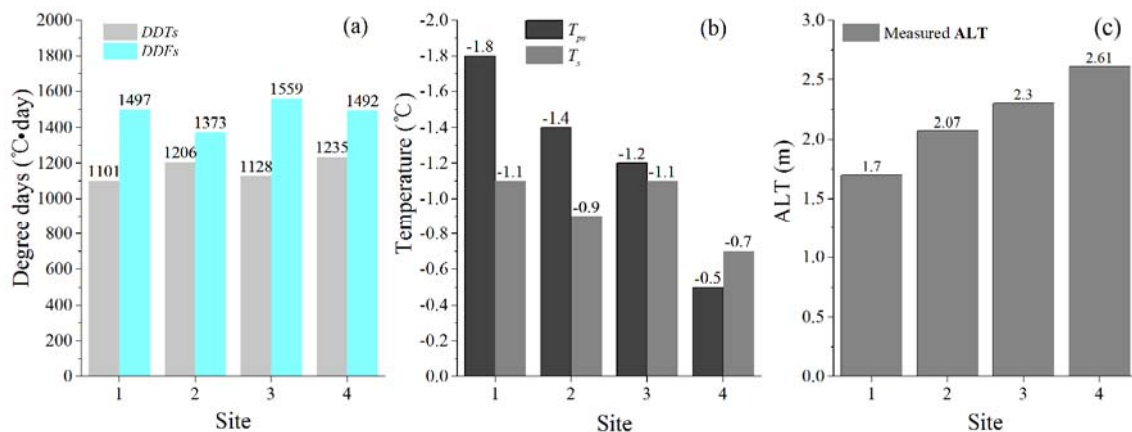


Figure 5 Measured mean data for the prediction equations. (a) presented the mean annual degree days at the four sites. (b) presented the mean annual ground surface temperature (T_s) and the mean annual temperature at the permafrost surface at the four sites. (c) showed the mean ALTs of all sites.

Table 3 Statistical analysis of calculated and measured T_{ps} (°C). ΔT (°C) is the mean difference between measured and calculated T_{ps} of each site. SD is the standard deviation of the calculated T_{ps}

Site	TTOP model				Kudryavtsev model			
	Mean value	SD	ΔT	Relative error (%)	Mean value	SD	ΔT	Relative error (%)
1	-1.54	0.52	0.26	14.2	-2.05	0.81	0.25	13.9
2	-1.06	0.51	0.14	11.4	-1.52	0.43	0.32	26.3
3	-1.18	0.42	0.02	2.1	-1.35	0.42	0.15	12.5
4	-0.45	0.12	0.05	10.1	-0.65	0.21	0.15	29.7

summary is shown in Table 4. Eq. 3 calculated the ALT more satisfactory than Eq. 4 did.

During the study period, the ALT calculated with Eq. 3 was 1.71 to 1.85 m for site 1, 1.91 m to 2.09 m for site 2, 2.13 m to 2.34 m for site 3 and 2.62 m to 2.84 m for site 4, respectively. The mean relative error for all sites from the modified Stefan model was less than 7%. Generally, the relative error of the standard Stefan model is 10% to 30% on the QTP (Xu et al. 2010). In contrast, Eq. 4 predicated the ALT was 2.14 m to 2.20 m at site 1, 2.24 m to 2.40 m at site 2, 2.42 m to 2.47 m at site 3 and 2.49 m to 2.59 m at site 4, respectively. Eq. 4 always overestimated the ALT by 0.13 m to 0.47 m for sites 1 to 3. At site 4, it underestimated the ALT by a mean value of 0.07 m. The mean relative error of Eq. 4 was below 30% for all sites.

4 Discussion

In most contemporary studies, ground temperatures are obtained and analyzed at a single point for each studied site (e.g. Riseborough et al. 2008). At a regional scale, macroscale proxy data may lead to overly generalized results, but at a local scale, models derived from point measurements may be difficult to apply at a regional scale (Janke et al. 2012). We measured ground temperatures with fine-scale grids at each site, and recorded notable within-site variations in ground temperatures (Figure 4). Intra-site variability leads to model uncertainty when conditions are applied at a larger scale. Models employed in this study combine both thermophysical and geographical capabilities and represent controlling factors of ALT and T_{ps} with limited number of site-specific parameters. All four study sites in Wudaoliang Basin are within an area of 800 m², and air temperature and topography are similar for all sites. Therefore, ground surface conditions and soil moisture conditions, which influence the soil thermal properties, seem to be

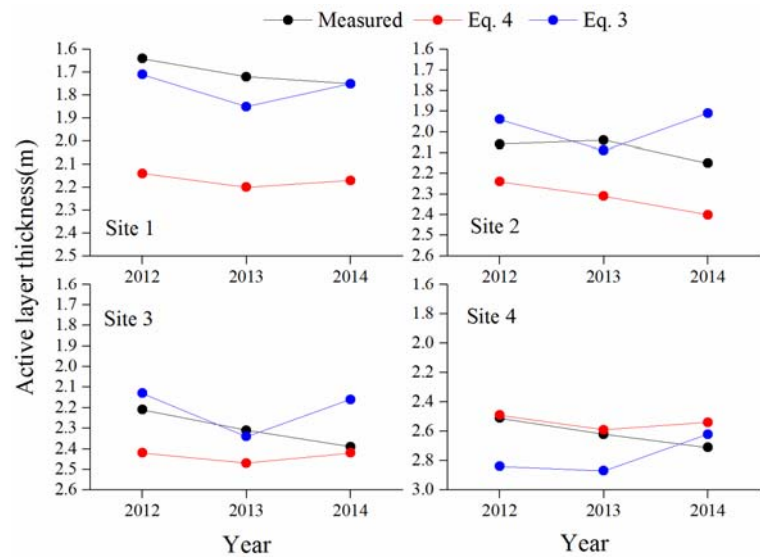


Figure 6 Comparisons of the ALTs between the measured and modeled values during the period of 2013 to 2014 at each site.

Table 4 Statistical analysis of calculated and measured ALT (m). Δ ALT (m) is the average difference between calculated and measured ALT. The values were all averaged from 2012 to 2014

Site	Mean measured ALT	Modified Stefan solution			Kudryavtsev model		
		Mean value	Δ ALT	Mean relative error (%)	Mean value	Δ ALT	Mean relative error (%)
1	1.70	1.77	0.07	3.9	2.17	0.47	27.4
2	2.08	1.98	0.10	4.9	2.32	0.23	11.2
3	2.30	2.21	0.09	4.1	2.44	0.13	5.8
4	2.61	2.78	0.16	6.3	2.54	0.07	2.8

primary factors that control T_{ps} and ALT.

4.1 Ground surface condition variables

In this study, averaged values from the boreholes at each sites were used as inputs to the models, however, the inter-annual spatial variability of the ground surface temperatures should not be ignored. Figure 4 indicates that the observed range of variability is up to 2.0°C at site 1, 2.6°C at site 2, 2.9°C at site 3 and 3.2°C at site 4. Similar spatial variability in ground surface temperature has been recorded recently in the Alps and Norway (Gisnås et al. 2014; Gubler et al. 2011; Pogliotti et al. 2015; Rödder and Kneisel 2012). The thermal effect of snow cover was the main control on variability in these other permafrost regions. For our study sites, the variability may be caused by heterogeneous ground surface conditions. Vegetation influenced the near-surface ground

temperatures by reducing solar radiation. At the same time, the vegetation may reduce evaporation and help maintain soil moisture. The rock grids may lower the wind speeds, and increase the albedo of the ground surface and heat conduction. Sand has a low specific heat capacity and high permeability, which promotes high heat absorption and release. Jin et al. (2008) and Lv et al. (2008) have reported on the combined influences of these local environmental variables on ground temperature on the QTP. Ground surface temperature variability could influence the near-surface ground temperatures and increase the uncertainty of the models. Figures 7 and 8 present the relation between measured T_{ps} and calculated T_{ps} based on Eq. 1 and Eq. 2, taking into account variability at sites. At site 3 and 4, T_{ps} from Eq. 1 and measured values corresponded well ($R^2 > 0.9$), but at site 1 and 2 there was more scatter ($R^2 < 0.3$). The difference between the T_{ps} calculated by the case with the averaged value (Sect. 3.2) and with the variability observed at the sites is up to 1°C. Riseborough (2007) studied the effect of transient conditions on the *TTOP* model and found that inter-annual variability does not influence the model results if long-term averages are used. Hence, averages of multi-year and repeated measurements can reduce the error of Eq. 1. Sazonova and Romanovsky (2003) compared the Eq. 2 results with measured temperatures from 32 sites in Siberia, and reported an accuracy of 0.2°C to 0.4°C and a good correlation between the T_{ps} values over a long time scale. This is similar to the results in our study (0.15°C to 0.25°C). Eq. 2 seems

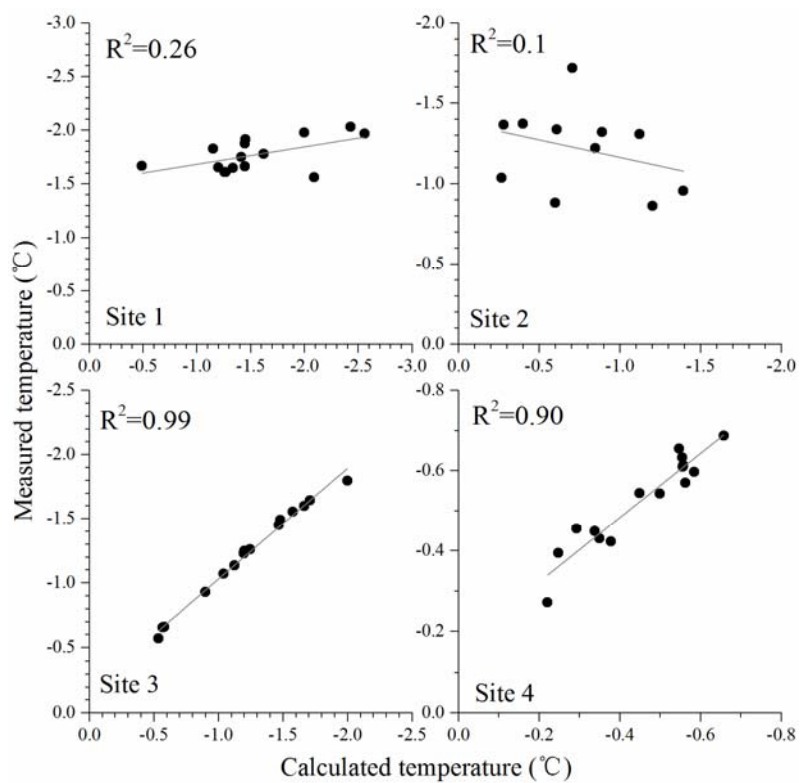


Figure 7 Relationship of the measured T_{ps} and calculated values from Eq. 1 of each borehole at the four sites.

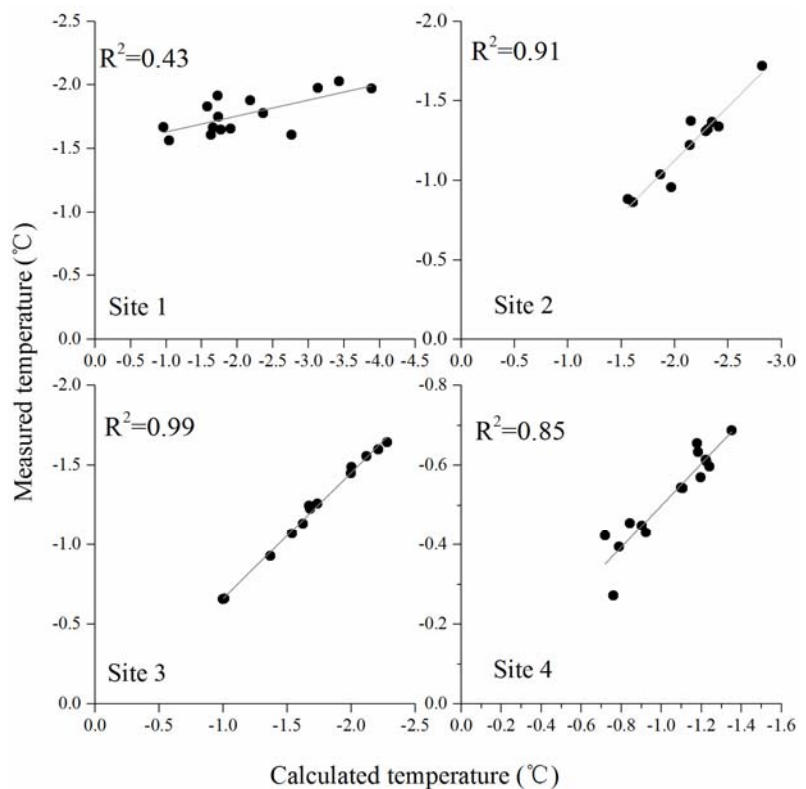


Figure 8 Relationship of the measured T_{ps} and calculated values from Eq. 2 in each borehole at the four sites.

insensitive to the variability of the ground surface temperature for all sites except at site 1 ($R^2 = 0.44$). Accounting for the temperature amplitudes (A_s) may be responsible for this because there was little A_s variability in all sites.

4.2 Soil thermal properties

The soil thermal properties mainly depend on the substrate's material composition (Kurylyk et al. 2015). Soil was divided into two major layers with distinct thermal properties at the study sites (Table 1). The near-surface soil type was similar among all sites. According to the measurements, soil moisture affected the thermal properties of the frozen and thawed soil and hydrological process. Heterogeneous soil thermal properties may therefore affect the model results.

Soil moisture content was measured over the summers during the study period at three depths in the soil profile. No data are reported here from winter because the moisture contents were outside of the sensor's measurement accuracy range. The soil was very dry close to the surface, especially at sites 3 and 4, where the volumetric water content was less than 0.1. Lin et al. (2015) reported a reversed thermal offset due to the arid conditions. Arid conditions may change the relation between thawed and frozen soil thermal conductivities. Evaporation and moisture percolation were also unrestricted in dry soils. Advective and convective heat transport plays an important role in regions of significant groundwater flow or vapor migration (Kurylyk et al. 2014). Data from the Wudaoliang Weather Station over the past 10 years indicates that precipitation is mainly concentrated between May and September. The annual precipitation was about 370 mm, however, the annual evaporation reached about 1421 mm similar to values of 1300 mm to 1500 mm reported by Wu and Zhang (2008). We hypothesized that the advective heat transport by rainfall and conductive heat transport increased the near surface ground temperature in summer. Future work will test this hypothesis by employing the algorithms (considering heat advection) which was studied in Kurylyk et al. (2014b).

4.3 Some other factors influencing the modeling

The four spatial models used to determine

ground temperature and ALT are one-dimensional models, so do not consider the lateral heat flow between adjacent points (Riseborough et al. 2008; Harris et al. 2009). Lateral heat flow may result from the spatial variability in soil properties and the ground water flow from the rivers or the lakes. Additional factors such as the unfrozen water content may have also influenced the modeling results. Therefore, monitoring of the groundwater conditions and heat transport is necessary so that the impact of non-conductive processes can be quantified and evaluated, if possible, by a sophisticated hydrological model accounting for water flow and heat transport.

Further research on intra-site variability in additional areas is necessary to gain a sound understanding of local factors controlling the thermal regime, and to assess the uncertainties of model application at the regional scale. Advanced measurement methods, such as geophysical investigations, multicriteria GIS, and remote sensing may help improve approximations of site parameters in the temporal and spatial domains.

5 Summary and Conclusions

We obtained detailed gridded ground temperatures and active-layer thicknesses measurements at four sites with different surface conditions in Wudaoliang Basin on the QTP. The measured values were compared with those produced by permafrost models over a period of 3 years. We concluded the following:

(1) There were notable differences in observed ground temperatures and active-layer thicknesses both within and among the sites. Ground surface condition and soil water content variations were mainly responsible for these differences. Lateral heat flow may also account for some of the variation.

(2) The TTOP model (Eq. 1) produced more accurate annual temperatures at the surface of permafrost than the Kudryavtsev model (Eq. 2), when averaged values were used. The relative error was below 15% for the TTOP model and 30% for the Kudryavtsev model in all sites.

(3) A modified Stefan solution (Eq. 3) produced better satisfactory accuracies than the Kudryavtsev model (Eq. 4) when estimating active-

layer thicknesses. The mean relative error of the modified Stefan solution was <7% for all sites. The Kudryavtsev model had a mean relative error of 2.8% to 27.4% for different ground surface conditions. Additionally, the Kudryavtsev model requires more input parameters than the Stefan solution does. The accuracy and practicability are limited. The modified Stefan solution may be applied to climate-changes studies in the future.

(4) Additional field investigations over longer periods focused on the interrelationships between permafrost thaw and hydrologic change are necessary. These efforts should employ advanced measurement methods to obtain adequate and extensive local parameters that will help improve model accuracy and benefit the application of

hydrological models.

Acknowledgments

This study was funded by the State Key Development Program of Basic Research of China (973 Plan, Grant No. 2012CB026101), the National Science and Technology Support Plan (Grant Nos. 2014BAG05B01, 2014BAG05B05). Constructive comments by two anonymous reviewers and the Editor led to significant improvements in this paper. We are also indebted to Brendan O'Neill, Department of Geography and Environmental Studies, Carleton University, for the final English editing.

References

- Cheng GD, Jin HJ (2013) Permafrost and groundwater on the Qinghai-Tibet Plateau and in northeast China. *Hydrogeology Journal* 21(1): 5-23. DOI: 10.1007/s10040-012-0927-2
- Ding YJ (1998) Recent degradation of permafrost in China and the response to climatic warming. Proceedings of the 7th International Conference of Permafrost, Yellowknife, Canada. pp 225-230.
- Fang HB, Zhao L, Wu XD, et al. (2015) Soil taxonomy and distribution characteristics of the permafrost region in the Qinghai-Tibet Plateau, China. *Journal of Mountain Science* 12(6): 1448-1459. DOI: 10.1007/s11629-014-3133-y
- Gisnäs K, Westermann S, Schuler TV, et al. (2014) A statistical approach to represent small-scale variability of permafrost temperatures due to snow cover. *The Cryosphere* 8(6): 2063-2074. DOI: 10.5194/tc-8-2063-2014
- Gubler S, Fiddes J, Keller M, et al. (2011) Scale-dependent measurement and analysis of ground surface temperature variability in alpine terrain. *The Cryosphere* 5(2): 431-443. DOI: 10.5194/tc-5-431-2011
- Harris C, Aronson LU, Christiansen HH, et al. (2009) Permafrost and climate in Europe: Monitoring and modelling thermal, geomorphological and geotechnical responses. *Earth Science Reviews* 92(3-4): 117-171. DOI: 10.1016/j.earscirev.2008.12.002
- Henry K, Smith M (2001) A model-based map of ground temperatures for the permafrost regions of Canada. *Permafrost and Periglacial Processes* 12(4): 389-398. DOI: 10.1002/ppp.399
- Janke JR, Williams MW, Evans JA (2012) A comparison of permafrost prediction models along a section of Trail Ridge Road, Rocky Mountain National Park, Colorado, USA. *Geomorphology* 138(1): 111-120. DOI: 10.1016/j.geomorph.2011.08.029
- Jin HJ, Sun L, Wang S, et al. (2008) Dual influences of local environmental variables on ground temperatures on the interior-eastern Qinghai-Tibet Plateau (I): Vegetation and snow cover. *Journal of Glaciology and Geocryology* 30(4):535-545. (In Chinese)
- Jin HJ, Wei Z, Wang S, et al. (2008) Assessment of frozen-ground conditions for engineering geology along the Qinghai-Tibet highway and railway, China. *Engineering Geology* 101(3-4): 96-109. DOI: 10.1016/j.enggeo.2008.04.001
- Jin HJ, Zhao L, Wang S, et al. (2006) Thermal regimes and degradation modes of permafrost along the Qinghai-Tibet Highway. *Science China Earth Sciences* 49(11): 1170-1183. DOI: 10.1007/s11430-006-2003-z
- Kudryavtsev VA, Garagulya LS, Melamed V (1977) Fundamentals of frost forecasting in geological engineering investigations, Nauka, Moscow. Draft translation 606. CRREL, Hanover, NH. pp 489.
- Kurylyk BL, Macquarrie KTB, Mckenzie JM (2014a) Climate change impacts on groundwater and soil temperatures in cold and temperate regions: Implications, mathematical theory, and emerging simulation tools. *Earth Science Reviews* 138: 313-334. DOI: 10.1016/j.earscirev.2014.06.006
- Kurylyk BL, Masaki H (2015) Improved stefan equation correction factors to accommodate sensible heat storage during soil freezing or thawing. *Permafrost and Periglacial Processes*. (<http://onlinelibrary.wiley.com/doi/10.1002/ppp.1865/pdf>, Accessed on 2015-9-30). DOI: 10.1002/ppp.1865
- Kurylyk BL, Mckenzie JM, Macquarrie KTB et al. (2014b) Analytical solutions for benchmarking cold regions subsurface water flow and energy transport models: One-dimensional soil thaw with conduction and advection. *Advances in Water Resources* 70(4): 172-184. DOI: 10.1016/j.advwatres.2014.05.005
- Li SX, Cheng GD (1996) The future thermal regime of numerical simulating permafrost on Qinghai-Xizang (Tibet) Plateau, China, under climate warming. *Science China Earth Sciences* 39(4): 434-441.
- Li X, Cheng GD (1999) A GIS-aided response model of high-altitude permafrost to global change. *Science China Earth Sciences* 42(1): 72-79. DOI: 10.1007/BF02878500
- Lin ZJ, Burn CR, Niu FJ, et al. (2015) The thermal regime, including a reversed thermal offset, of arid permafrost sites with variations in vegetation cover density, Wudaoliang Basin, Qinghai-Tibet Plateau. *Permafrost and Periglacial Processes* 26(2): 142-159. DOI: 10.1002/ppp.1840
- Luo DL, Jin HJ, Marchenko S, et al. (2014) Distribution and changes of active layer thickness (ALT) and soil temperature (TTOP) in the source area of the Yellow River using the GIPL

- model. *Science China Earth Sciences* 57(8): 1834-1845. DOI: 10.1007/s11430-014-4852-1
- Lv, LZ, Jin HJ, Wang S (2008) Dual influence of local environmental variables on ground temperatures on the Interior-Eastern Qinghai-Tibet Plateau (II): Sand-layer and surface water bodies. *Journal of Glaciology and Geocryology* 30(4): 546-555. (In Chinese)
- Pogliotti P, Guglielmin M, Cremonese E, et al. (2015) Warming permafrost and active layer variability at Cime Bianche, Western European Alps. *The Cryosphere* 9(2): 647-661. DOI: 10.5194/tc-9-647-2015
- Riseborough D (2002) The mean annual temperature at the top of permafrost, the TTOP model, and the effect of unfrozen water. *Permafrost and Periglacial Processes* 13(2): 137-143. DOI: 10.1002/ppp.418
- Riseborough D (2007) The effect of transient conditions on an equilibrium permafrost-climate model. *Permafrost and Periglacial Processes* 18(1): 21-32. DOI: 10.1002/ppp.579
- Riseborough D, Shiklomanov N, Etzelmüller B, et al. (2008) Recent advances in permafrost modelling. *Permafrost and Periglacial Processes* 19(2): 137-156. DOI: 10.1002/ppp.615
- Romanovsky V, Osterkamp T (1997) Thawing of the active layer on the coastal plain of the Alaskan Arctic. *Permafrost and Periglacial Processes* 8(1): 1-22. DOI: 10.1002/ppp.579
- Rödder T, Kneisel C (2012) Influence of snow cover and grain size on the ground thermal regime in the discontinuous permafrost zone, Swiss Alps. *Geomorphology* 175-176: 1176-1189. DOI: 10.1016/j.geomorph.2012.07.008
- Sazonova T, Romanovsky V (2003) A model for regional-scale estimation of temporal and spatial variability of active layer thickness and mean annual ground temperatures. *Permafrost and Periglacial Processes* 14(2): 125-139. DOI: 10.1002/ppp.449
- Smith M, Riseborough D (1996) Permafrost monitoring and detection of climate change. *Permafrost and Periglacial Processes* 7(4): 301-309. DOI: 10.1002/(SICI)1099-1530(199610)7:4<301:AID-PPP231>3.0.CO;2-R
- Smith M, Riseborough D (2002) Climate and the limits of permafrost: a zonal analysis. *Permafrost and Periglacial Processes* 13(1): 1-15. DOI: 10.1002/ppp.410
- Van Everdingen RO (1998) Multi-language glossary of permafrost and related ground-ice terms. International Permafrost Association/ National Snow and Ice Data Center, University of Colorado, Boulder.
- Vaughan DG, Comiso JC, Allison J, et al. (2013) Observations: Cryosphere. *Climate Change 2013: The physical science basis. Contribution of working group I to the Fifth Assessment Report of the Intergovernmental Panel on climate change.* Cambridge University Press, Cambridge, United Kingdom and New York, USA. pp 362.
- Wilhelm KR, Bockheim JG, Kung S (2015) Active layer thickness prediction on the Western Antarctic Peninsula. *Permafrost and Periglacial Processes* 26(2): 188-199. DOI: 10.1002/ppp.1845
- Wu QB, Zhang TJ (2010) Changes in active layer thickness over the Qinghai-Tibetan Plateau from 1995 to 2007. *Journal of Geophysical Research Atmospheres* 115(D09107): 1-12. DOI: 10.1029/2009JD012974
- Wu QB, Zhang TJ (2008) Recent permafrost warming on the Qinghai-Tibetan Plateau. *Journal of Geophysical Research Atmospheres* 113(D13108): 1-22. DOI: 10.1029/2007JD009539
- Wu TH, Wang QB, Watanabe M, et al. (2008) Mapping vertical profile of discontinuous permafrost with ground penetrating radar at Nalaikh depression, Mongolia. *Environmental Geology* 56(8): 1577-1583. DOI: 10.1007/s00254-008-1255-7
- Wang SX (1993) Permafrost changes along with the Qinghai-Xizang Highway during the last decades. *Arid Land Geography* 16(1): 1-8. (In Chinese)
- Xie CW, Zhao L, Wu TH, et al. (2012) Changes in the thermal and hydraulic regime within the active layer in the Qinghai-Tibet Plateau. *Journal of Mountain Science* 9(4): 483-491. DOI: 10.1007/s11629-012-2352-3
- Xu XZ, Wang JD, Zhang LX (2010) Physics of frozen soils. Science Press, Beijing, China. pp 85-89. (In Chinese)
- Yang MX, Nelson FE, Shiklomanov NI, et al. (2010) Permafrost degradation and its environmental effects on the Tibetan Plateau: A review of recent research. *Earth Science Reviews* 103(1): 31-44. DOI: 10.1016/j.earscirev.2010.07.002
- Zhang TJ, Barry RG, Knowles K, et al. (1999) Statistics and characteristics of permafrost and ground-ice distribution in the Northern Hemisphere. *Polar Geography* 31(1): 132-154. DOI: 10.1080/10889370802175895
- Zhao L, Wu QB, Marchenko SS, et al. (2010) Thermal state of permafrost and active layer in Central Asia during the international polar year. *Permafrost and Periglacial Processes* 21(2): 198-207. DOI: 10.1002/ppp.688